of study will continue to play a key role in the characterization of the surface of honeycomb films that affect cell adhesion. Other interface characterization techniques using spectroscopy, microscopy, and diffraction would provide additional information and extend our understanding of the role of honeycomb film surfaces. Since the mechanisms involved in the cellular response to topography are quite complex, further research is required to elucidate the influence of a honeycomb-patterned surface on the biochemical pathways and cellular signaling mechanism that regulate cell adhesion and functions. This complete understanding of cell–material surface interactions will pave the way for successful implantation of biomaterials.

4. CONCLUSIONS

ECs were cultured on the honeycomb films in order to investigate the influence of the honeycomb pattern and the pore size on cell behavior. Honeycomb films exert a strong influence on cell morphology, proliferation, cytoskeleton, focal adhesion, and ECM production profiles. Our studies demonstrated that the cellular behaviors are controlled by the pore size of the honeycomb film. ECs showed increased spreading and flattening on the honeycomb film and expressed proper EC-specific functions. The focal adhesions existed locally along the intracellular edge of the elongated cells on the flat film. However, on the honeycomb film, the focal adhesions were localized along the edge of the pores distributed over the entire projected cell area. The honeycomb film with a pore size of 5 μm showed the highest number of focal adhesions. This implies that a higher focal adhesion density may induce a complex signal transduction for EC proliferation and functions. Fabrication of honeycomb films by self-organization would be an effective method that does not require lithography or consume a large amount of energy. The technology for fabricating 3-D honeycomb films with well-controlled pore sizes may be useful for constructing porous films with controlled pore sizes to improve cell performance. *In vivo* application of honeycomb films as a small diameter tubular scaffold is currently under evaluation; it may be an effective strategy for vascular tissue engineering.[43]

Acknowledgments: This work is supported by Grants-in-Aid and CREST from Japan Science and Technology Corporation (JST) and Special Coordination Funds for Promoting Science and Technology of Ministry of Education, Culture, Sports, Science and Technology.

References and Notes

1. L. G. Cima, J. P. Vacanti, and C. Vacanti, *J. Biomech. Eng.* 113, 143 (1991).
2. L. G. Griffith, B. Wu, and M. J. Cima, *Ann. N.Y. Acad. Sci.* 831, 382 (1997).
3. A. G. Mikos, Y. Bao, and L. G. Cima, *J. Biomed. Mater. Res.* 27, 183 (1993).
4. C. S. Chen, M. Mrksich, S. Huang, G. M. Whitesides, and D. E. Ingber, *Science* 276, 1425 (1997).
5. P. Clark, S. Britland, and P. Connolly. *J. Cell Sci.* 105, 203 (1993).
6. M. C. Wake, P. K. Gupta, and A. G. Mikos. *Cell Transplantation* 5, 465 (1996).
7. L. D. Harris, B. S. Kim, and D. J. Mooney, *J. Biomed. Mater. Res.* 42, 396 (1998).
8. L. Kam, W. Shain, J. N. Turner, and R. Bizios, *Biomaterials* 22, 1049 (2001).
9. J. Tan and W. M. Saltzman, *Biomaterials* 23, 3215 (2002).
10. J. B. Recknor, J. C. Recknor, D. S. Sakaguchi, and S. K. Mallapragada, *Biomaterials* 25, 2753 (2004).
11. S. J. Hollister, *Nat. Mater.* 4, 518 (2005).
12. N. Maruyama, T. Koito, J. Nishida, T. Sawadaishi, X. Cieren, K. Ijiro, O. Karthaus, and M. Shimomura, *Thin Solid Films* 327/329, 854 (1998).
13. O. Karthaus, N. Maruyama, X. Cieren, M. Shimomura, H. Hasegawa, and T. Hashimoto, *Langmuir* 16, 6071 (2000).
14. M. Shimomura and T. Sawadaishi, *Curr. Opin. Colloid Interf. Sci.* 6, 11 (2001).
15. K. Sato, M. Tanaka, K. Hasebe, M. Takebayashi, K. Nishikawa, T. Kawai, M. Matsushita, S. Todo, and M. Shimomura, *Int. J. Nanosci.* 1, 689 (2002).
16. T. Nishikawa, R. Ookura, J. Nishida, K. Arai, J. Hayashi, N. Kurono, T. Sawadaishi, M. Hara, and M. Shimomura, *Langmuir* 18, 5734 (2002).
17. H. Yabu, M. Tanaka, K. Ijiro, and M. Shimomura, *Langmuir* 19, 6297 (2003).
18. M. Tanaka, M. Takebayashi, M. Miyama, J. Nishida, and M. Shimomura, *Bio-Med. Mater. Eng.* 14, 439 (2004).
19. A. Tsuruma, M. Tanaka, N. Fukushima, and M. Shimomura, *e-J. Surf. Sci. Nanotechnol.* 3, 159 (2005).
20. H. Yabu, M. Takebayashi, M. Tanaka, and M. Shimomura, *Langmuir* 21, 3235 (2005).
21. J. Nemoto, Y. Uraki, T. Kishimoto, Y. Sano, R. Funada, N. Obata, H. Yabu, M. Tanaka, and M. Shimomura, *Bioresource Technol.* 96, 1955 (2005).
22. Y. Fukuhira, E. Kitazono, T. Hayashi, H. Kaneko, M. Tanaka, M. Shimomura, and Y. Sumi, *Biomaterials* 27, 1797 (2006).
23. M. Tanaka, K. Nishikawa, H. Okubo, H. Kamachi, T. Kawai, M. Matsushita, S. Todo, and M. Shimomura, *Colloids Surf. A* 284–285, 464 (2006).
24. A. Tsuruma, M. Tanaka, S. Yamamoto, N. Fukushima, and M. Shimomura, *Colloids Surf. A* 284–285, 470 (2006).
25. A. Curtis and C. Wilkinson, *Biomaterials* 18, 1573 (1997).
26. X. Jiang, S. Takayama, X. Qian, E. Ostuni, H. Wu, N. Bowden, P. LeDuc, D. Ingber, and G. M. Whitesides, *Langmuir* 18, 3273 (2002).
27. H. S. Nalwa (ed.), Handbook of Nanostructured Biomaterials and Their Applications in Nanobiotechnology, American Scientific Publishers, Los Angeles (2005), Vols. 1–2.
28. M. S. Baguneid, A. M. Seiflian, H. J. Salacinski, D. Murray, G. Hamilton, and M. G. Walker, *Br. J. Surg.* 93, 282 (2006).
29. S. Nishimura and K. Yamada, *J. Am. Chem. Soc.* 119, 10555 (1997).
30. P. Uttayarat, G. K. Toworfe, F. Dietrich, P. I. Lelkes, and R. J. Composto, *J. Biomed. Mater. Res.* 75, 668 (2005).
31. A. Hall, *Science* 279, 509 (1998).
32. D. E. Ingber, *Proc. Natl. Acad. Sci. USA* 87, 3579 (1990).
33. R. Singhvi, A. Kumar, G. P. Lopez, G. N. Stephanopoulos, D. I. C. Wang, G. M. Whitesides, and D. E. Ingber, *Science* 264, 696 (1994).
34. A. J. Garcia, M. D. Vega, and D. Boettiger, *Mol. Biol. Cell.* 10, 785 (1999).

35. N. Pernodet, M. Rafailovich, J. Sokolov, D. Xu, N. L. Yang, K. McLeod, *J. Biomed. Mater. Res.* 64, 648 (**2003**).
36. M. Arnold, A. Cavalcanti-Adam, R. Glass, J. Blümmel, W. Eck, M. Kantlehner, H. Kessler, and J. P. Spatz, *Chem. Phys. Chem.* 5, 383 (**2004**).
37. N. D. Gallant, K. E. Michael, and A. J. García, *Mol. Biol. Cell* 16, 4329 (**2005**).
38. J. D. Andrade (ed.), Surface and Interfacial Aspects of Biomedical Polymers, Plenum Publishers, New York (**1985**), p. 1.
39. M. Tanaka, A. Mochizuki, N. Ishii, T. Motomura, and T. Hatakeyama, *Biomacromolecules* 3, 36 (**2002**).
40. M. Tanaka and A. Mochizuki, *J. Biomed. Mater. Res.* 68A, 684 (**2004**).
41. S. Yamamoto, M. Tanaka, H. Sunami, S. Yamashita, Y. Morita, and M. Shimomura, *Surf. Sci.* 600, 3785 (**2006**).
42. H. Sunami, E. Ito, M. Tanaka, S. Yamamoto, and M. Shimomura, *Colloids Surf A* 284–285, 548 (**2006**).
43. M. Tanaka, Patent pending (JP2005-281268).

Received: 12 March 2006. Accepted: 22 May 2006.

RESEARCH ARTICLE

Available online at www.sciencedirect.com
SCIENCE DIRECT®
ELSEVIER
Colloids and Surfaces A: Physicochem. Eng. Aspects 284–285 (2006) 464–469
COLLOIDS AND SURFACES A
www.elsevier.com/locate/colsurfa

Control of hepatocyte adhesion and function on self-organized honeycomb-patterned polymer film

Masaru Tanaka[a,b,*], Kazutaka Nishikawa[c], Hisashi Okubo[d], Hirofumi Kamachi[d], Tomoaki Kawai[d], Michiaki Matsushita[b,d], Satoru Todo[b,d], Masatsugu Shimomura[b,e]

[a] *Creative Research Initiative "Sousei" (CRIS), Hokkaido University, Kita-Ku N21W10, Sapporo 001-0021, Japan*
[b] *CREST, Japan Science and Technology Corporation (JST), Honchou 4-1-8, Kawaguchi 332-0012, Japan*
[c] *Graduate School of Science, Hokkaido University, Kita-Ku N11W6, Sapporo 001-0021, Japan*
[d] *Graduate School of Medicine, Hokkaido University, Kita-Ku N15W7, Sapporo 060-8638, Japan*
[e] *Nanotechnology Research Center, Research Institute for Electronic Science, Hokkaido University, Kita-Ku N21W10, Sapporo 001-0021, Japan*

Received 31 July 2005; received in revised form 26 November 2005; accepted 29 November 2005
Available online 9 February 2006

Abstract

Hepatocytes were cultured on a honeycomb-patterned polymer film (honeycomb film) formed by self-organization in order to investigate the influence of the honeycomb pattern on cell behavior. The changes in cell morphologies and actin filaments were observed by optical, fluorescence, and scanning electron microscopy. Hepatocytes were flattened, and the actin filaments appeared conspicuously in the spreading regions on a flat film. In contrast, the hepatocytes that were cultured on the honeycomb film were observed to form a spherical shape, and the actin filaments were localized inside the edge of the spheroid. The spheroids were observed within several hours after seeding on the honeycomb film; they were attached and the spheroid shape was maintained without any deformation. The spheroids expressed a higher level of liver specific function than the cell monolayers on the flat film. These results suggest that the honeycomb film is a suitable material for tissue engineering scaffolds and biomedical devices.

Keywords: Cell adhesion; Hepatocyte; Self-organization; Hepatic function; Cell surface interaction

1. Introduction

The design of nano- and microstructures by self-organization is one of the most important issues for creating new materials. This design has a variety of potential applications in tissue engineering scaffolds. The scaffolds must provide suitable substrates for cell adhesion, proliferation, and differentiated function [1–4]. Porous polymer materials have been investigated and are widely used in biomedical applications such as tissue engineering and artificial organs. These porous materials have been fabricated by many methods [5–14], including lithography, micro-contact printing, phase separation, solution casting/salt leaching, freeze-immersion, emulsion freeze-drying, gel casting, gas forming, and colloidal assemblies as templates. These techniques are certainly useful in the fabrication of the porous materials. However, these techniques require a large amount of energy and involve many processes. In addition, there is a limited variety of materials available for scaffolds. The preparation of honeycomb films by casting a polymer solution on solid substrates has been previously reported [15–23]. This method has a great advantage in that the films can be prepared with ease, at a low cost, and with less limitation of materials for scaffolds.

One of the key issues in liver tissue engineering and the development of bioartificial liver assist devices is the design of an effective porous polymer scaffold for hepatocyte adhesion and hepatic function. However, it is difficult to control hepatocyte adhesion and enhance the hepatic function in vitro, and the hepatocyte activities are often limited by the lack of the liver specificity of the environment. In this study, we describe the fabrication of highly regular porous surfaces (honeycomb films) formed by a solution casting technique under humid air condi-

* Corresponding author.
E-mail address: tanaka@poly.es.hokudai.ac.jp (M. Tanaka).

0927-7757/$ – see front matter © 2005 Elsevier B.V. All rights reserved.
doi:10.1016/j.colsurfa.2005.11.098

tion, and the culture of hepatocytes on these films in order to investigate cell adhesion and function.

2. Experimental

2.1. Materials

A copolymer of dodecylacrylamide and ω-carboxyhexylacrylamide as shown in Fig. 1a was used as an emulsifier in this study. The copolymer was synthesized by the previously reported method [24]. The copolymer is amphiphilic because the polymer forms a stable monolayer at the air–water interface. The copolymer is abbreviated as Cap in this study. The molecular weight of the polymer, which was estimated by size exclusion chromatography, is 4.5×10^4 g/mol. The water was purified by a Millipore system (Milli-Q, Millipore). Organic solvents and other chemicals were commercially available and were used without further purification.

2.2. Preparation of honeycomb and flat films

The honeycomb film was prepared on a glass substrate by the method described previously [15–23]. Briefly, Cap was dissolved in chloroform at a concentration of 5 g/L. The polymer solution was poured into a round glass dish (9.3 cm in diameter) under blowing highly humid air (1.0 L/min). The Cap flat film was prepared as follows. The Cap solution (5 g/L) was dropped onto a slide glass. The cover glass with the polymer layer was spun at 1000 rpm for 30 s by using a spin coater (1H-7D, Mikasa).

2.3. Hepatocyte cell culture

Using a modified two-step collagenase perfusion technique in situ, hepatocytes were isolated from 6- to 7-week-old male Wistar rats weighing 200–300 g [25]. The obtained cells were washed four times by centrifugation at 50 × *g* for 1 min. The hepatocyte viability was determined by trypan blue exclusion. The hepatocytes were cultivated in serum-free Williams' E medium supplemented with 0.1 μM $CuSO_4 \cdot 5H_2O$ (Wako Pure Chemical Industries Ltd., Osaka, Japan), 25 nM Na_2SeO_3 (Wako), 1.0 μM $ZnSO_4 \cdot 7H_2O$ (Wako), 0.1 μM insulin (Sigma Chemicals Co., St. Louis, MO), 1.0 μM dexamethasone (Sigma), 20 ng/mL epidermal growth factor (Sigma), 100 μg/mL ascorbic acid diphosphate (Sigma), 5 KIE/mL aprotinin (Bayer, Germany), 48 μg/mL gentamicin (Schering-Plough, USA), and 100 ng/mL chloramphenicol (Sankyo, Japan). The cell suspension of the hepatocytes was adjusted to the cell density of 2.0×10^5 cells/well (24-well plates) in Williams' E medium. The hepatocytes were seeded onto polymer substrates that were immersed in the medium for over 6 h. They were then incubated at 37 °C in 95% air containing 5% CO_2. The culture medium exchange was carried out every 24 h. The morphologies of hepatocytes after seeding were observed using a phase contrast microscope (IX 70, Olympus).

2.4. Scanning electron microscopic observation

The cells that were cultured 72 h after seeding were fixed in 2% glutaraldehyde in phosphate-buffered saline (PBS) (Wako) overnight at 4 °C. After washing three times with PBS, each sample was fixed in 1.0% osmium tetroxide (Wako) aqueous solution for 1 h and was rinsed in PBS. Subsequently, the samples were dehydrated by washing in increasing ethanol concentrations and then air-dried. The samples were transferred to microporous specimen capsules and dried by means of a critical point dryer (HCP-2, Hitachi Co., Tokyo, Japan). The dried samples were mounted on aluminum stages by double stick tape and coated with palladium gold (approximately 5 nm of coating) by using an ion sputter coater (E-1030, Hitachi). All samples were observed using a scanning electron microscope (SEM) (S-3500N, Hitachi).

2.5. Actin staining and confocal laser scanning microscopy

The actin filaments in the hepatocytes that were cultured 72 h after seeding were stained. After washing with PBS, the cells were fixed with 3.7% formaldehyde for 30 min at room temperature. The cells were washed twice with PBS and permeabilized for 15 min with 0.1% Triton X-100 (Sigma) and 1.0% bovine serum albumin (Sigma) in PBS. After rinsing twice with PBS, the cells were stained for 30 min with rhodamine-phalloidin (Molecular Probes, Eugene, OR) in PBS at room temperature. The stained cells were then rinsed four times with PBS and immersed for 1 h at the fourth rinse. All samples were removed to slides. Coverslips were applied onto the samples and sealed with manicure. The confocal laser scanning microscope (CLSM) (MRC-1024, Bio-Rad Laboratories Inc., Hercules, CA) was utilized for observation. The Zeiss Plan-Neofluar 40×/0.75 NA objective lens was used to visualize the actin filaments. The

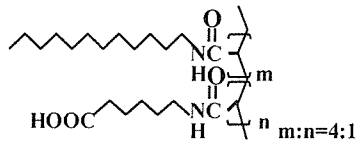

(a) **Amphiphilic polymer (Cap)**

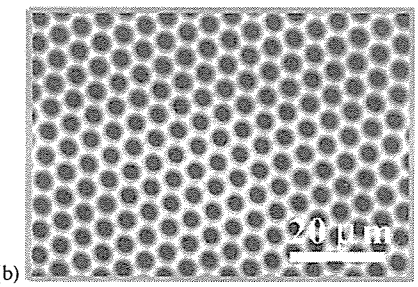

(b)

Fig. 1. Chemical structure of a copolymer of dodecylacrylamide and ω-carboxyhexylacrylamide (Cap) and SEM image of a honeycomb film.

excitation wavelength was set to 568 nm, and a 585 nm long-pass filter was utilized to collect the emitted light. Images were acquired using LaserSharp software (version 3.2, Bio-Rad Laboratories Inc.).

2.6. Urea synthesis

Urea concentration was measured by the diacetyl monoxime method [26]. The culture medium was replaced with Williams' E medium containing 5 mM NH_4Cl, and the hepatocytes were cultivated in this medium with ammonia for 2 h. The samples cultivated in this medium were removed from the well and stored separately at −40 °C.

2.7. DNA content

To assess the number of hepatocytes, the DNA contents of the cultured hepatocytes were measured by 4′, 6-diamidino-2-phenylindole (DAPI) fluorometry using calf thymus DNA as a standard [27]. The cells were detached from the dish by adding protease and incubating them at 37 °C for 1 h. The cell pellets were suspended in a solution containing 50 mM Tris–Cl, 0.1 M NaCl, and 5 mM edetic acid and then homogenized using an ultrasonic homogenizer (Branson Sonifier 250, Branson Sonic Power Co., Danbury, CT). Following the addition of 100 ng/mL DAPI, the fluorescence of the solution was measured with a spectrofluorophotometer (RF-510; Shimadzu, Kyoto, Japan). All samples of the DNA were stored at −40 °C. The data on the measurement of urea and DNA concentration were expressed as mean ± SD, and statistical analysis was performed using ANOVA. A P value of less than 0.05 was considered statistically significant.

3. Results and discussion

3.1. Honeycomb film

The honeycomb-patterned surface showed a highly regular hexagonal arrangement of holes with a pore size of 5 μm (Fig. 1b). The condensation of water from the air occurred due to evaporation cooling when a water-immiscible solvent was used. The self-packed and monodispersed water droplets formed on the solution surface acted as a temporary template of the pores. In general, the condensed water droplets are not stable and eventually start coalescing. In order to prepare the highly regular porous (honeycomb-patterned) film, the stabilization of the water droplets is necessary. The role of the amphiphilic polymer in the pattern formation is to prevent the fusion of the water droplets. Cap (Fig. 1a) as a surfactant contributes to stabilized the water droplets at the polymer solution and water interface. As a result, the water droplets are prevented from fusing to each other by the intervening the amphiphilic polymer layer. Most of polymers dissolved in water-immiscible solvent can be fabricated to the (honeycomb-patterned film by the addition of Cap. Various experimental factors affect the pore structures. The pore size can be controlled in the range of 100 nm to 50 μm by changing the casting conditions [15–23]. Unlike other template or lithographic methods, the advantage of this method is the ease with which such patterned surfaces can be created using various materials without large energy consumption.

3.2. Morphologies of adhered hepatocytes on honeycomb and flat films

Most tissue-derived cells are anchorage dependent and require attachment to a solid surface for viability and growth. Therefore, the initial events that occur when a cell approaches a surface are of fundamental interest. In tissue engineering, cell adhesion to a surface is critical because adhesion precedes other events, such as cell spreading, cell migration, and differentiated cell functions.

The viability of hepatocytes prepared from rat liver was 90–95%. Fig. 2 shows the time course of the morphologies of adhered hepatocytes on both flat and honeycomb films observed using a phase contrast microscope. Seventy-two hours after culture, the morphologies of adhered hepatocytes on both films were observed using SEM (Fig. 3). The morphology of hepatocytes on the honeycomb film was compared with that of hepatocytes on the flat film. The morphologies of hepatocytes on both films were observed to be different. On the flat film, the hepatocytes appeared to have a typical monolayer morphology (Fig. 2a). The hepatocytes on the flat film had already attached themselves to the film surface at 6 h, and cell spreading and nuclei were observed subsequently. The attached hepatocytes were observed to form a spreading morphology known as monolayer at 24 h. This monolayer had extended sufficiently at 72 h (Figs. 2a and 3a). The flat film possesses an adhesive property because the monolayer appears on a substrate that has this property, such as tissue culture polystyrene dish or collagen coated dish.

Another typical morphology of hepatocyte spheroids was observed on the honeycomb film (Figs. 2b and 3b). Although the hepatocytes on the honeycomb film had already attached themselves to the film surface in a manner identical to those on a flat film at 6 h, cell spreading and flattening of the nuclei were rarely demonstrated. The honeycomb film restricted cell spreading, but did not inhibit cell adhesion. The attached hepatocytes were gathered gradually. The spheroids then outgrew gradually in the culture, and an increase in the mean size of the spheroids was observed with time (0–12 h). Rapid spheroid formation became possible, and the spheroids could be fixed on the honeycomb film. The size of the spheroids was maintained after 24 h at approximately 100 μm, and deformation and detachment of the spheroids from the honeycomb film were not observed. This behavior is expected to exhibit better and longer hepatic function. It should be noted that both the flat and honeycomb films were prepared from the same polymer. This implies that the topological property of the honeycomb film affected the formation of hepatocyte morphology. The honeycomb film may be appropriate for the regulation of the degree of cell–cell versus cell–material interactions, and the honeycomb pattern variations can also affect liver specific functions.

The mechanism of the interaction between the hepatocytes and the honeycomb film require further investigation. However,

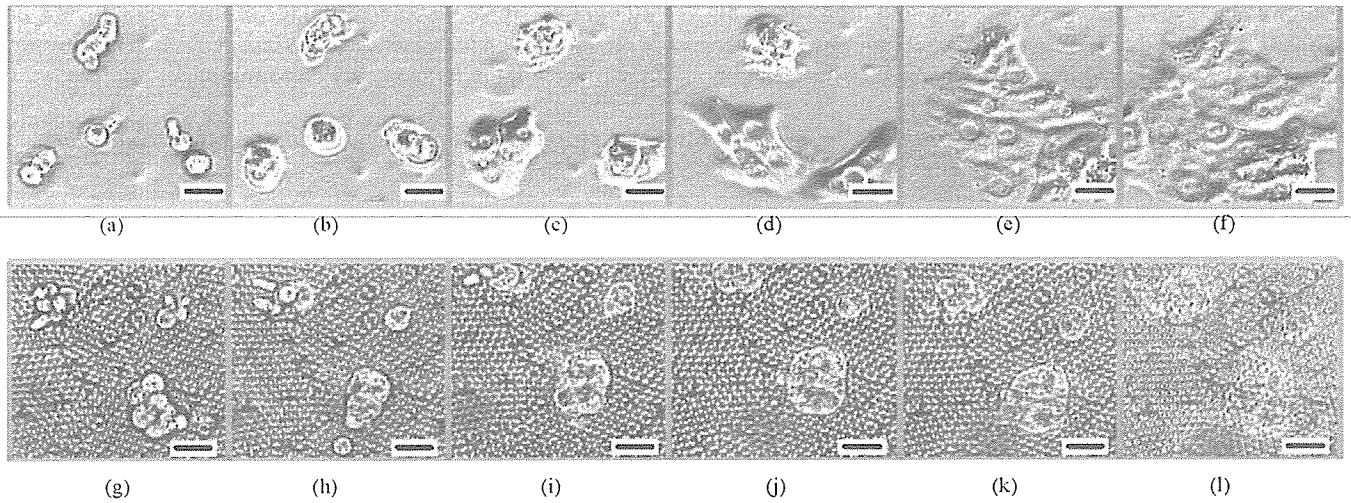

Fig. 2. Time course of the morphologies of hepatocytes in phase contrast images on flat film at (a) 6 h, (b)12 h, (c) 24 h, (d) 36 h, (e) 48 h, and (f) 72 h; and on honeycomb film at (g) 6 h, (h) 12 h, (i) 24 h, (j) 36 h, (k) 48 h, and (l) 72 h after culture. These images were obtained from the same view field (bar: 50 μm).

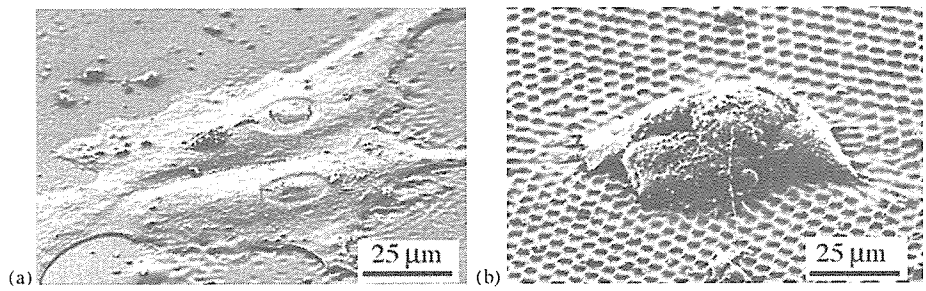

Fig. 3. SEM images of hepatocytes 72 h after culture on (a) flat film and (b) honeycomb film.

the strategy of immobilization and stabilization of hepatocyte sheroids through the use of honeycomb films would prove advantageous in the design of a bioartificial liver assist device, where the hepatocytes could attach themselves to a film with a high surface area, maintain their functions, and remain stable against the perfusion and shear forces in the bioreactor.

3.3. Actin filaments

Cytoskeletal actin is known as a liner protein that forms the shape of cells. In addition, it is important even in functional expressions such as proliferation and migration. These events involve the development of specific intercellular adhesions and redistribution of cell–cell and cell–material adhesion forces, which are intimately related to the dynamic cytoskeletal organization.

Fig. 4 shows CLSM images of actin filaments in adhered hepatocytes on both flat and honeycomb films. The actin filaments appeared conspicuously in the spreading regions of the hepatocytes on the flat film (Fig. 4a). Although the actin filaments in the cytoplasm could not be seen at 24 h, they were observed in great amounts of fibrous actin at 72 h (Fig. 4a), while the actin filaments existed locally in the intracellular edge with the forming morphology in which the cells overlapped the

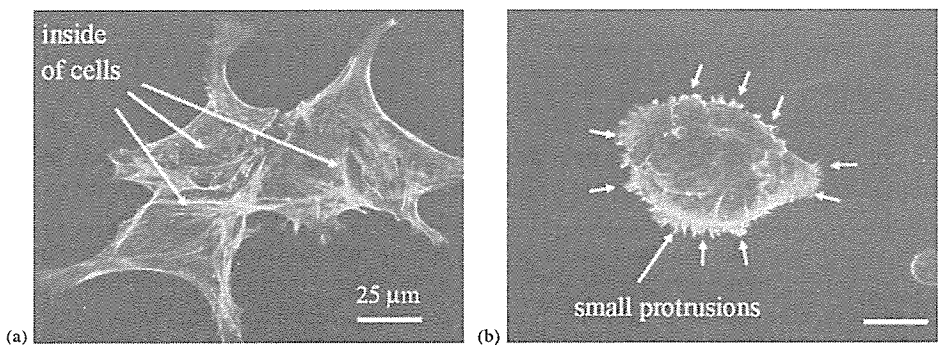

Fig. 4. CLSM images of actin localization in adhered hepatocytes at 72 h after culture on (a) flat film and (b) honeycomb film.

spheroids on the honeycomb film (Fig. 4b). Small protrusions were observed around the spheroids, and the actin filament was localized along the protrusions (Fig. 4b). These results indicated that the honeycomb film could control hepatocyte adhesion following cytoskeletal protein production.

The results obtained in this study increase the interest in the Rho family of small GTPase. The Rho family has emerged as the key regulator of the actin cytoskeleton and it coordinates the control of cellular activities, such as gene transcription and adhesion [28]. It is possible that the topological properties of the honeycomb film affected signal transduction with the Rho family, since morphology and actin localization of hepatocytes on the honeycomb film were different from those on the flat film.

3.4. Urea synthesis

The hepatocyte morphology and formation of actin filaments are important factors that affect the hepatocyte function. Spheroidal aggregates of hepatocytes, or hepatocyte spheroids, are known to exhibit better and longer hepatocyte functions than hepatocytes produced by monolayer culture [29], and they are expected to be a promising candidate for the main bioreactor component of hybrid artificial livers. Next, we investigated liver specific functions.

Fig. 5 shows the data on urea synthesis profiles 72 h after culture on both the flat and honeycomb films. The urea level in the hepatocytes cultured on the honeycomb film was higher than that of the hepatocytes cultured on the flat film. As mentioned above, the result indicated that urea synthesis reflected the hepatocyte morphology since it was known that an interaction between morphology and functions results in spheroids with differentiated functions that are higher than those of monolayer hepatocytes. It was considered that hepatocytes on the honeycomb film were formed as tissue-like structures, and the high expression of urea synthesis appeared accordingly. Thus, the enhancement and maintenance of hepatic function for a long period of time may be possible by utilizing the honeycomb film.

We found that the honeycomb-patterned structure quite affected not only cell adhesion but also actin organization and urea synthesis of the hepatocytes. These results indicate that the physical properties of films should be considered in the cases where porous films were used as scaffolds. To date, there is little information on porous-film-induced topological effects on hepatocytes, although an optimal balance between the degree of cell–cell and cell–material interactions has been recognized as a critical factor for guiding three-dimensional cellular organization and improving hepatic function on porous films for tissue engineering scaffolds [10,30].

The honeycomb film is also a useful tool for obtaining insights into the mechanism of cell–cell and cell–material interactions, which is one of the central research topics in nanobiotechnology. At present, the mechanism by which the cells recognize the honeycomb film in cultures is not clear. It is generally known that adhesion and morphology of cells are influenced by the variety and structure of adsorbed proteins on the material surface [31]. We have reported the adsorbed proteins and water structure on polymer in order to clarify the main factor that causes cell–material and protein–material interactions [32–48]. Future investigation will focus on the factor causing the honeycomb-film-induced changes in the morphologies and functions of hepatocytes in terms of hepatocyte adhesion receptors and focal adhesion that involve hepatocyte intercellular signal transduction and gene expression.

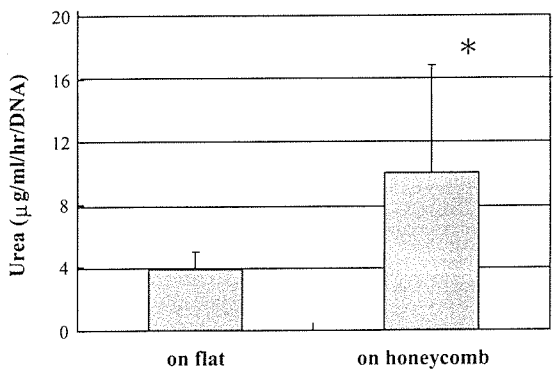

Fig. 5. Urea synthesis of hepatocytes 72 h after culture on flat and honeycomb films. ($^*p < 0.05$ vs. flat, mean ± standard deviation, $n = 6$).

4. Conclusions

Honeycomb films have a strong influence on cell adhesion, actin organization, and hepatic function. The hepatocytes on flat films exhibited greater cell spreading and flattening; however, they did not express appropriate liver specific functions. In contrast, the hepatocytes that were cultured on the honeycomb film formed a spherical shape and enhanced the hepatic function. The fabrication of honeycomb films by self-organization can become an effective method that does not require lithography and large energy consumption. The honeycomb films can be potentially applied in tissue engineering scaffolds and biomedical devices.

Acknowledgements

This study is supported by grants-in-aid from Japan Science and Technology Corporation (JST) and Special Coordination Funds for Promoting Science and Technology.

References

[1] L.G. Cima, J.P. Vacanti, C. Vacanti, J. Biomech. Eng. 113 (1991) 143–151.
[2] L.G. Griffith, B. Wu, M.J. Cima, Ann. N.Y. Acad. Sci. 831 (1997) 382–397.
[3] A.G. Mikos, Y. Bao, L.G. Cima, J. Biomed. Mater. Res. 27 (1993) 183–189.
[4] C.S. Chen, M. Mrksich, S. Huang, G.M. Whitesides, D.E. Ingber, Science 276 (1997) 1425–1427.
[5] P. Clark, S. Britland, P. Connolly, J. Cell Sci. 105 (1993) 203–212.
[6] L. Kam, W. Shain, J.N. Turner, R. Bizios, Biomaterials 22 (2001) 1049–1054.
[7] J. Tan, W.M. Saltzman, Biomaterials 23 (2002) 3215–3225.
[9] J.B. Recknor, J.C. Recknor, D.S. Sakaguchi, S.K. Mallapragada, Biomaterials 25 (2004) 2753–2767.
[10] A.G. Mikos, A.J. Thorsen, L.A. Czerwonka, Y. Bao, R. Langer, D.N. Winslow, J.P. Vacanti, Polymer 35 (1994) 1068–1077.

[11] M.C. Wake, P.K. Gupta, A.G. Mikos, Cell Transplant. 5 (1996) 465–473.
[12] A.T. Gutsche, H. Lo, J. Zurlo, J. Yager, K.W. Leong, Biomaterials 17 (1996) 387–393.
[13] L.D. Harris, B.S. Kim, D.J. Mooney, J. Biomed. Mater. Res. 42 (1998) 396–402.
[14] Y.S. Nam, J.J. Yoon, T.G. Park, J. Biomed. Mater. Res. 53 (2000) 1–7.
[15] N. Maruyama, T. Koito, J. Nishida, T. Sawadaishi, X. Cieren, K. Ijiro, O. Karthaus, M. Shimomura, Thin Solid Films 327–329 (1998) 854–856.
[16] O. Karthaus, N. Maruyama, X. Cieren, M. Shimomura, H. Hasegawa, T. Hashimoto, Langmuir 16 (2000) 6071–6076.
[17] M. Shimomura, T. Sawadaishi, Curr. Opin. Colloid. Interface Sci. 6 (2001) 11–16.
[18] K. Sato, M. Tanaka, K. Hasebe, M. Takebayashi, K. Nishikawa, T. Kawai, M. Matsushita, S. Todo, M. Shimomura, Int. J. Nanosci. 1 (2002) 689–693.
[19] T. Nishikawa, R. Ookura, J. Nishida, K. Arai, J. Hayashi, N. Kurono, T. Sawadaishi, M. Hara, M. Shimomura, Langmuir 18 (2002) 5734–5739.
[20] H. Yabu, M. Tanaka, K. Ijiro, M. Shimomura, Langmuir 19 (2003) 6297–6300.
[21] M. Tanaka, M. Takebayashi, M. Miyama, J. Nishida, M. Shimomura, Bio-med. Mater. Eng. 14 (2004) 439–445.
[22] A. Tsuruma, M. Tanaka, N. Fukushima, M. Shimomura, J. Surf. Sci. Nanotech. 3 (2005) 159–164.
[23] H. Yabu, M. Takebayashi, M. Tanaka, M. Shimomura, Langmuir 21 (2005) 3235–3237.
[24] S. Nishimura, K. Yamada, J. Am. Chem. Soc. 119 (1997) 10555–10556.
[25] P.O. Seglen, Methods Cell Biol. 13 (1976) 29–83.
[26] W.H. Marsh, B. Fingerhut, H. Miller, Clin. Chem. 11 (1965) 624–627.
[27] C.F. Brunk, K.C. Jones, T.W. James, Anal. Biochem. 92 (1979) 497–500.
[28] A. Hall, Science 279 (1998) 509–514.
[29] J. Landry, D. Bernier, C. Ouellet, R. Goyett, N. Marceau, J. Cell Biol. 101 (1985) 914–923.
[30] C.S. Ranucci, A. Kumar, S.P. Batra, P.V. Moghe, Biomaterials 21 (2000) 783–793.
[31] J.D. Andrade, in: J.D. Andrade (Ed.), Surface and Interfacial Aspects of Biomedical Polymers, Plenum Publishers, New York, 1985, p. 1.
[32] M. Tanaka, T. Motomura, M. Kawada, T. Anzai, Y. Kasori, T. Shiroya, K. Shimura, M. Onishi, A. Mochizuki, Biomaterials 21 (2000) 1471–1481.
[33] M. Tanaka, T. Motomura, M. Kawada, T. Anzai, Y. Kasori, T. Shiroya, K. Shimura, M. Onishi, A. Mochizuki, Y. Okahata, Jpn. J. Artif. Organs. 9 (2000) 209–216.
[34] M. Tanaka, T. Motomura, N. Ishii, K. Shimura, M. Onishi, A. Mochizuki, T. Hatakeyama, Polym. Int. 49 (2000) 1709–1713.
[35] H. Kitano, K. Ichikawa, M. Fukuda, A. Mochizuki, M. Tanaka, J. Colloid Surface Sci. 242 (2001) 133–140.
[36] K. Ichikawa, T. Mori, H. Kitano, M. Fukuda, A. Mochizuki, M. Tanaka, J. Polym. Sci., B Polym. Phys. 39 (2001) 2175–2182.
[37] M. Tanaka, A. Mochizuki, T. Motomura, K. Shimura, M. Onishi, Y. Okahata, Colloids Surf. A. 193 (2001) 145–152.
[38] M. Tanaka, A. Mochizuki, T. Shiroya, T. Motomura, K. Shimura, M. Onishi, Y. Okahata, Colloids Surf. A. 203 (2002) 195–204.
[39] M. Tanaka, A. Mochizuki, N. Ishii, T. Motomura, T. Hatakeyama, Biomacromolecules 3 (2002) 36–41.
[40] M. Ide, T. Mori, K. Ichikawa, H. Kitano, M. Tanaka, A. Mochizuki, H. Oshiyama, W. Mizuno, Langmuir 19 (2003) 429–435.
[41] S. Ye, S. Morita, G. Li, H. Noda, M. Tanaka, K. Uosaki, M. Osawa, Macromolecules 36 (2003) 5694–5703.
[42] M. Tanaka, A. Mochizuki, J. Biomed. Mater. Res. 68A (2004) 684–695.
[43] G. Li, S. Morita, S. Ye, M. Tanaka, M. Osawa, Anal. Chem. 76 (2004) 788–795.
[44] H. Kitano, T. Mori, Y. Takeuchi, S. Tada, M. Gemmei-ide, Y. Yokoyama, M. Tanaka, Macromol. Biosci. 5 (2005) 314–321.
[45] J. Nemoto, Y. Uraki, T. Kishimoto, Y. Sano, R. Funada, N. Obata, H. Yabu, M. Tanaka, M. Shimomura, Bioresour. Technol. 96 (2005) 1955–1958.
[46] H. Kitano, S. Tada, T. Mori, K. Takaha, M. Gemmei-Ide, M. Tanaka, M. Fukuda, Y. Yokoyama, Langmuir 21 (2005) 11932–11939.
[47] E. Hirota, K. Ute, M. Uehara, T. Kitayama, M. Tanaka, A. Mochizuki, J. Biomed. Mater. Res. 76A (2006) 550–560.
[48] Y. Fukuhira, E. Kitazono, T. Hayashi, H. Kaneko, M. Tanaka, M. Shimomura, Y. Sumi, Biomaterials 27 (2006) 1797–1802.

Available online at www.sciencedirect.com
SCIENCE DIRECT®
ELSEVIER
Colloids and Surfaces A: Physicochem. Eng. Aspects 284–285 (2006) 470–474
COLLOIDS AND SURFACES A
www.elsevier.com/locate/colsurfa

Topographical control of neurite extension on stripe-patterned polymer films

Akinori Tsuruma [a], Masaru Tanaka [b,c,*], Sadaaki Yamamoto [b,c], Nobuyuki Fukushima [d], Hiroshi Yabu [c,e], Masatsugu Shimomura [c,e]

[a] *Graduate School of Science, Hokkaido University, Kita-Ku N10W8, Sapporo 060-0810, Japan*
[b] *Creative Research Initiative "Sousei" (CRIS), Hokkaido University, Kita-Ku N21W10, Sapporo 001-0021, Japan*
[c] *CREST, Japan Science and Technology Corporation (JST), Honchou 4-1-8, Kawaguchi 332- 0012, Japan*
[d] *Graduate School of Medicine, Hokkaido University, Kita-Ku N15W7, Sapporo 060-8638, Japan*
[e] *Nanotechnology Research Center, Research Institute for Electronic Science, Hokkaido University, Kita-Ku N21W10, Sapporo 001-0021, Japan*

Received 31 July 2005; received in revised form 25 November 2005; accepted 29 November 2005
Available online 7 February 2006

Abstract

Controlling cell responses to material surfaces is important for tissue engineering. Topographical property on material surfaces can play a crucial role in directing nerve regeneration. We prepared regular stripe-patterned (groove-ridge pattern) polymer film by self-organization in order to control direction of neurite extension. Neural cells from cerebral cortex of embryonic day-14 mice were cultured on the film coated with poly-L-lysine. Here, we describe a complex and unusual contact guidance dependent on the pattern feature size. The neurites grew perpendicular to wide groove of 12.7 μm and wide ridge of 4.3 μm but parallel to narrow grooves (6.1 and 8.4 μm) and narrow ridge (2.2 and 3.6 μm). The neurites sprouted parallel to the narrow groove but uniformly on the wide groove. The emersion of neurites was suppressed and the length of neurites was longer compared with on a flat film. These results are of interest to understanding contact guidance and designing scaffold for neural network formation.

Keywords: Neuron; Micro-patterning; Self-organization; Tissue engineering; Contact guidance

1. Introduction

The central nervous system (CNS) fails to recover following nerve injuries or neurodegenerative diseases. Clinical therapies for CNS damages need surgical end-to-end connection or implantation of conduit materials [1]. A variety of biomaterials have been investigated for neural tissue engineering application. Synthetic materials such as fiber or hydrogels have been used to expand neurites and reconstruct neural network [2,3]. It has been reported that topography of micro-grooves on surface can control direction of neurite outgrowth and neurite development (contact guidance) [4–9]. This surface-contact guidance of neurites on topographical pattern is important to design devices in neural regeneration and to understand axonal formation [9]. The application of micro-fabrication techniques to the topographic designing of polymer surface can provide valuable information for understanding of the contact guidance and materials for neural tissue engineering [10–12]. In previous studies, micro-patterned surfaces were fabricated by lithography and micro-contact printing [13–16]. These techniques are expected to be applied for neural regeneration in the future. However, the techniques require high energy and involve many processes. In addition, materials for scaffolds applicable to the techniques are limited.

We have reported that regular patterns can be formed by casting diluted polymer solution on solid substrates [17–20]. This method has great advantage that the films can be prepared with ease, low-cost and no limitation of materials for scaffold. In this study, we prepared stripe-patterned polymer films on a solid substrate by the method previously reported [20] and cultured neural cells from cerebral cortex of embryonic day-14 mice on the film coated with poly-L-lysine to investigate how these films influence neuronal morphologies and neurite extension in cultures.

* Corresponding author.
E-mail address: tanaka@poly.es.hokudai.ac.jp (M. Tanaka).

0927-7757/$ – see front matter © 2005 Elsevier B.V. All rights reserved.
doi:10.1016/j.colsurfa.2005.11.100

2. Experiment

2.1. Preparation of stripe-patterned polymer films

Stripe-patterned polymer films were prepared with an instrument described in the previous literature (Fig. 1) [20,21]. We prepared poly (ε-caprolactone)/chloroform solution (1 g/L) before casting. Glass plates were overlapped by ca. 4 cm and separated with a narrow gap (200 μm). Then, polymer solution (200 μl) was injected into the gap between two glass plates. The upper glass plate was moved straightly at the velocity controlled from 60 to 100 μm/s (Fig. 1). A thin liquid film of polymer solution was continuously formed from the edge of sliding glass, and the polymer intermittently deposited on the bottom glass following evaporation of solvent at the meniscus. Polymer patterns were observed by optical microscope (BH-2, Olympus, Japan), atomic force microscope (SPA-400, Seiko Instruments, Japan) and scanning electron microscope (S-3500, Hitachi, Japan).

2.2. Preparation of flat polymer films

The polymer solution (poly(ε-caprolactone) (MW 30,000–70,000)/chloroform solution (1 g/L)) was dropped onto a slide glass. The slide glass with polymer layer was spined at 1000 rpm for 30 s by spin coater (MIKASA, 1H-7D).

2.3. Neural cell culture

Neural cells were prepared from the cerebral cortex of embryonic day-14 mice (CLEA Japan, Inc). In brief, the cerebral cortices of embryonic day-14 mice were dissected and the meninges were carefully removed. The tissues were transferred to 15 ml tubes with culture medium containing 55 μM 2-mercaptoethanol and gently triturated with a fire-polished pasteur pipette until most of the tissues were dissociated into single cells. Then, the cell number and viability were measured. The cells were seeded onto the flat film to estimate the population of neural stem cells (NSCs). The neural cells were seeded onto the flat and stripe patterned film at a density of 2.0×10^4 cells/cm^2. They were cultured in serum medium (Opti-MEM (Invitrogen), 10% fetal bovine serum, and 55 μM 2-mercaptoethanol (Invitrogen)) for the first day at 37 °C under a humidified atmosphere of 5% CO_2. After the second day, they were further cultured in serum-free medium (Opti-MEM, B27 supplement, and 55 μM 2-mercaptoethanol). After 5 days culture, morphologies of neurons and neurite extension were observed using scanning electron microscope (SEM) (S-3500, Hitachi, Japan), confocal laser scanning microscope (CLSM) (Fluoview FV 300, Olympus, Japan) and phase contrast microscope (IX 70, Olympus, Japan).

2.4. Preparation of the sample for SEM observation

The cultured cells were fixed with 2.5% glutaraldehyde in phosphate-buffered saline (PBS). They were washed with PBS and water. Subsequently, the samples were dehydrated by washing in increasing ethanol concentrations and then air-dried. The samples were sputtered with platinum.

2.5. Preparation of the sample for CLSM observation

The cultured cells were fixed with 10% formaldehyde in PBS for 30 min at room temperature. The samples were washed with PBS three times for 5 min. They were then incubated in blocking solution (5% goat serum, 0.2% Triton X-100 in PBS) for 1 h. Then, the samples were incubated with mouse monoclonal anti-β-tubulin III (1:500) in PBS for 2 h. After washing with PBS, the samples were incubated with fluorescein isothiocyanate (FITC)-conjugated anti-mouse IgG (1:200) for 2 h. After washing with

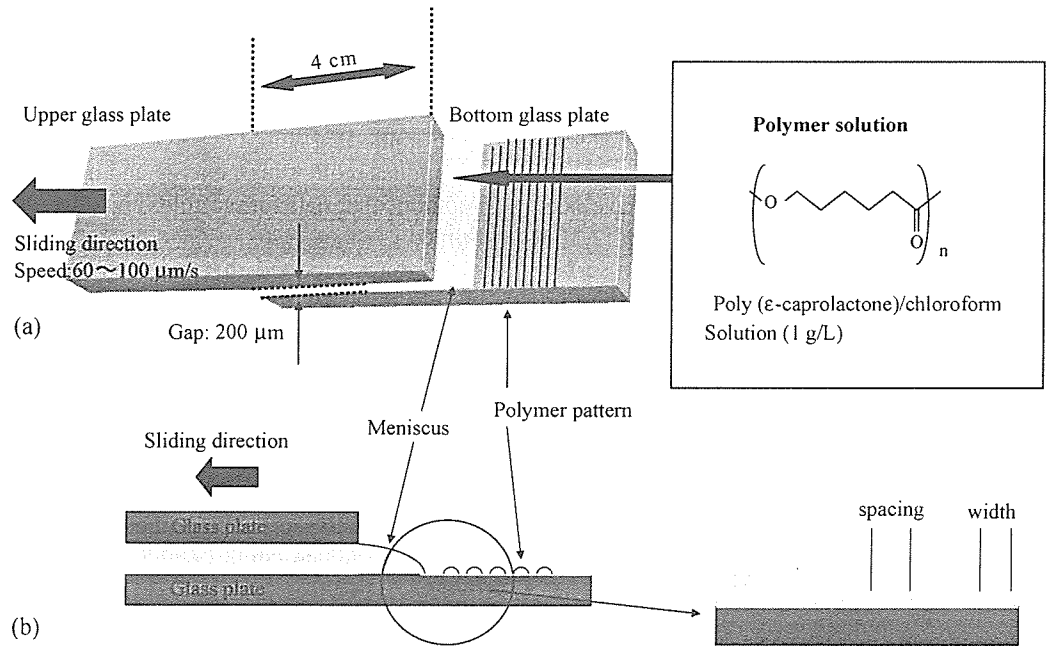

Fig. 1. Schematic images for preparation of stripe-patterned films. (a) Tilt and (b) side view.

PBS and water, the sample were air-dried and then mounted with mounting media for CLSM observation.

3. Results and discussion

3.1. Stripe-patterned polymer films

At a sliding speed of 60, 70 and 100 μm/s, the stripe pattern polymer films were prepared. Width ("ridge") and spacing ("groove") of the substrates were 2.2 and 6.1 μm (sliding speed: 60 μm/s), 3.6 and 8.4 μm (sliding speed: 70 μm/s), and 4.3 and 12.7 μm (sliding speed: 100 μm/s), respectively. The height of the ridges was in the range of 50–100 nm. This type of the periodic deposition is caused by "stick-slip motion," which is often observed in colloidal crystals [22] and is commonly known as the coffee stain phenomenon [23]. Due to evaporation of solvent at the meniscus, polymer was condensed at the edge of solution [20,21]. Increasing local viscosity of polymer solution caused by polymer gelation resulted in pinning of the solution edge at the meniscus. After complete deposition of polymer onto the glass substrate, the pinning stress relaxed and the solution edge moved in the sliding direction like a receding tide until the next pinning.

3.2. Morphologies of neurons and neurites extension on patterned/flat films

Fig. 2 shows morphologies of neurons and extended neurites observed by using SEM, and CLSM. Cells cultured for 5 days on the flat and patterned films were stained with neuron-specific marker, β-tubulin III. Cells were positive for β-tubulin III on the both films, indicating that these cultured cells were differentiated neurons (Fig. 2a and c).

The large difference was noted when comparing the behavior and morphology of neurons on the flat film with those on the patterned films. On the flat film, neurons were round in shape. They extended many branched neurites, and seemed to form neuronal network with random direction of neurite outgrowth (Fig. 2a and b). In contrast, on the patterned film, neurons attached and elongated parallel to the stripes (indicated by arrowheads in Fig. 2c and d). Cells altered their shapes, orientation and direction of neurites extension to align with the stripe-pattern (indicated by arrows in Fig. 2c and d). These results imply that the stripe-pattern affects the orientation of neurite outgrowth, neurite emersion and neurite growth.

3.3. Effect of pattern width ("ridge") and spacing ("groove")

Next, we describe the effects of width ("ridge") and spacing ("groove") of the stripe-patterned polymer film on neurites extension. The morphologies on the patterned films showed complex and unusual contact guidance dependent on the pattern feature size (Figs. 2c and d, 3a and b). Neurites were predicted to be able to extend out of the grooves with height ≤4.7 μm [5]. Unless the neurites are able to extend out of

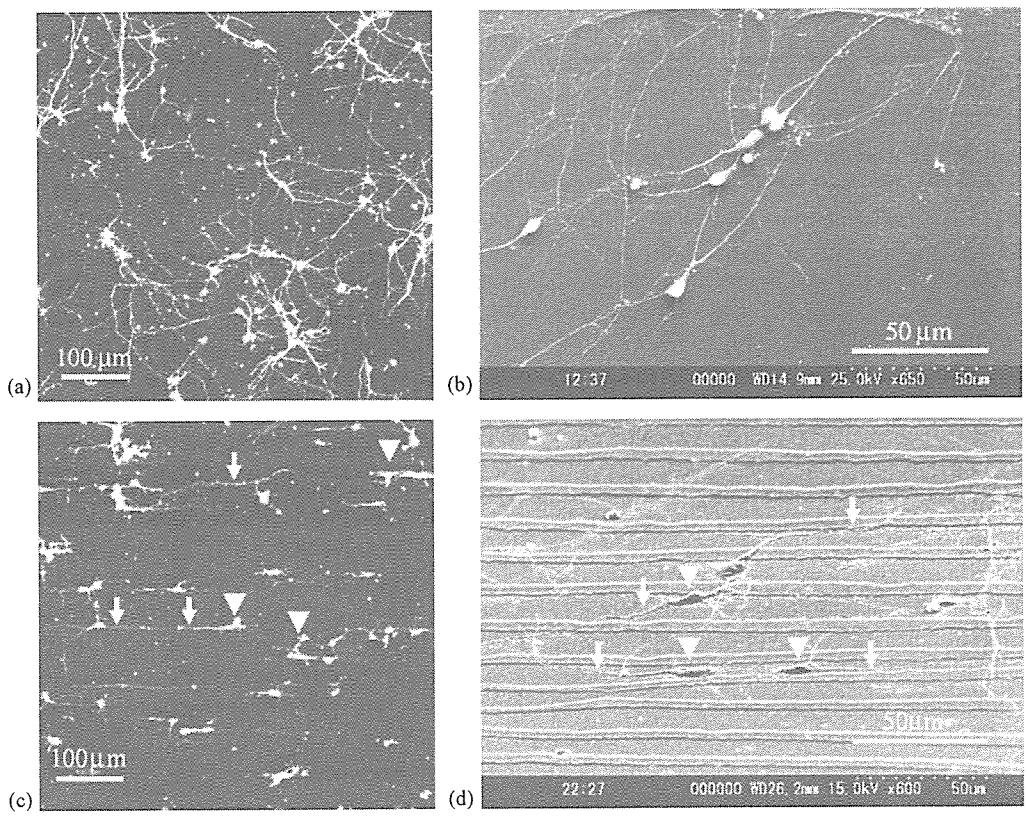

Fig. 2. Morphologies of neurons and neurite extension in SEM and CLSM. (a) Fluorescence image on flat film (staining for β-tubulinIII), (b) SEM image on flat film, (c) fluorescence image on stripe-patterned film (staining for β-tubulinIII) width: 3.6 μm, spacing: 8.4 μm (sliding speed: 70 μm/s) and (d) SEM image on stripe-patterned film. width: 3.6 μm, spacing: 8.4 μm (sliding speed: 70 μm/s).

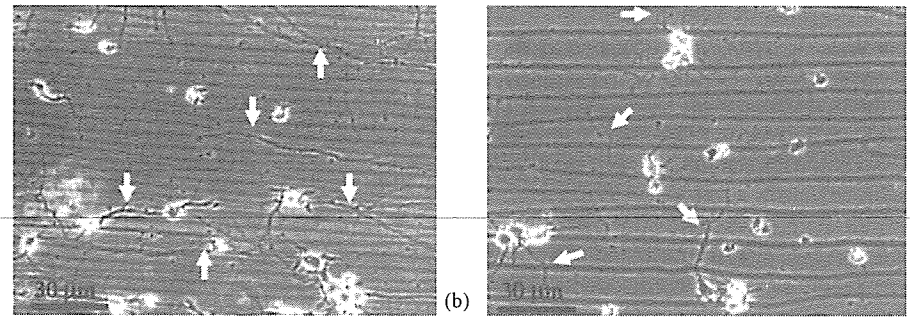

Fig. 3. Morphologies of neurons and neurite extension in phase contrast images on (a) stripe-patterned film, width: 2.2 μm, spacing: 6.1 μm (sliding speed: 60 μm/s) and (b) stripe-patterned film, width: 4.3 μm, spacing: 12.7 μm (sliding speed: 100 μm/s).

the grooves of the stripe-patterned film, a subset of neurons extended neurites in grooves parallel to the axis of the pattern on narrow pattern width and spacing (width: 2.2 μm, spacing: 6.1 μm) (indicated by arrows in Fig. 3a). The narrow patterns determine the site on a cell body where neurites emerged (Fig. 2c and d, and 3a). On wide pattern width and spacing (width: 4.3 μm, spacing: 12.7 μm), most neurites extended across the axis of the pattern (indicated by arrows in Fig. 3b). The number of neurites per a cell body was reduced and the length of neurites was longer on the stripe patterned-films comparing with that on the flat film shown in Fig. 2a and b. These results show that the neurites sense the dimension of regular stripe patterns.

In previous studies, similar parallel and perpendicular contact guidance of neurites has been observed on microgrooved fused quartz substrates in response to stripe-patterned feature dimension and cells. Several hypothesis have been proposed on the mechanism of contact guidance. CNS neuroblasts orient their neurites both perpendicular and parallel to the axis of grating-like structure [4]. Perpendicular orientation is frequently observed when the microstructured grooves have depths between 300 and 800 nm and a width of 1 μm. Embryonic rat hippocampal neurites grow parallel to grooves with height of 1 μm and width of 4 μm, and perpendicular to grooves with height of 130 nm and width of 1 μm on fused quarz [5,6]. *Xenopus* neurites grow parallel to grooves as shallow as 14 nm and as narrow as 1 μm [5]. Recently, neonatal rat dorsal root ganglion neuron was reported to extend neurites that bridged across grooves with no underlying solid support on deep grooves of 50 μm [7]. The cell–cell interaction was supposed to be involved in the bridging of the neurites across grooves. Not only groove width but also ridge width plays an important role in bridge formation. The dependence of contact guidance on the pattern size for neurons from cerebral cortex of embryonic day-14 mice in the present study conflicts that for CNS neuroblasts and embryonic rat hippocampal neurons. The pattern width (ridge width) of the stripe-patterned polymer film in the present study varied companying with the spacing. The neurites might sense both the pattern width and spacing. This might lead to the contact guidance characteristic for the stripe-patterned polymer films by self-organization different from that on microgrooved fused quartz.

The possibilities considered for the mechanism of the perpendicular orientation were proposed such as the extension of a neurite at right angles to the structure by recognition of the physical surface structure of neurite bundles and the involvement of more specific surface molecules on the neurites responsible for the perpendicular contact guidance [4]. Parallel and perpendicular orientation of hippocampal neurites are supposed to utilize different mechanisms [6]. Growth cones of neurite recognize the topography of the surfaces [13,23,24]. The structure of growth cones is critical to neurite guidance and aids in the sensing and exploration of the underlying environment. Further, stripe-geometry influences cytoskeletal arrangement and focal adhesion formation of neurons and growth cones that determine signal transduction associated with directional neurite growth [25–27]. The stripe-pattern topographies may produce ridge-groove-ridge signals dependent on the pattern dimension that direct growth cone attachment leading to producing oriented and directed growth. The mechanisms by which cells sense stripe-patterned surface contours and translate them into directional growth remains, however, still largely unexplored and are not entirely clear. Our study extends the studies previously reported to indicate that a stripe-pattern determines the growth direction and length of neurites, and the number of neurites per cell depending on the wide of groove and ridge, leading to comprehensive interpretation on the response of neurons to stripe-patterned surface in future.

4. Conclusions

Stripe-patterned polymer films were effective for orientation of neurites extension. Orientation of neurites depended on the pattern width and spacing. These biodegradable patterned films can be used as patterned polymer biomaterials for implants in living body. Patterning of polymers by self-organization can become an effective method for modification of neural implants and contribute to develop regenerative medicine [28–30].

Acknowledgements

This study is supported by Grants-in-Aid from Japan Science and Technology Corporation (JST) and Special Coordination Funds for Promoting Science and Technology.

References

[1] P. Lu, L.L. Jones, E.Y. Snyder, M.H. Tuszynski, Exp. Neulo. 181 (2003) 115–129.
[2] G.A. Silva, C. Czeisler, K.L. Niece, E. Beniash, D.A. Harrington, J.A. Kessler, S.I. Stupp, Science 303 (2003) 1352–1355.
[3] F. Yang, R. Murugan, S. Wang, S. Ramarkrishna, Biomaterials 26 (2005) 2603–2610.
[4] I. Nagata, A. Kawana, N. Nakatsuji, Development 117 (1993) 401–408.
[5] A.M. Rajnicek, S. Britland, C.D. McCaig, J. Cell Sci. 110 (1997) 2905–2913.
[6] A.M. Rajnicek, C.D. McCaig, J. Cell Sci. 110 (1997) 2915–2924.
[7] J.S. Goldner, J.M. Bruder, G. Li, D. Gazzola, D. Hoffman-Kim, Biomaterials 27 (2006) 460–472.
[8] W. Ma, Q.Y. Liu, D. Jung, P. Manos, J.J. Pancrazio, A.E. Schaffner, J.L. Barker, D.A. Stenger, Dev. Brain Res. 111 (1998) 231–243.
[9] J.D. Foley, E.W. Grunwald, P.F. Nealey, C.J. Murphy, Biomaterials 26 (2005) 3639–3644.
[10] A. Tsuruma, M. Tanaka, N. Fukushima, M. Shimomura, e-J. Surf. Sci. Nanotech. 3 (2005) 159–164.
[11] A. Tsuruma, M. Tanaka, N. Fukushima, M. Shimomura, Kobunshi Ronbunshu 61 (2004) 628–633.
[12] J.B. Recknor, D.S. Sakaguchi, S.K. Mallapragada, Ann. N.Y. Acad. Sci. 1049 (2005) 24–27.
[13] P. Clark, S. Britland, P. Connolly, J. Cell Sci. 105 (1993) 203–212.
[14] L. Kam, W. Shain, J.N. Turner, R. Bizios, Biomaterials 22 (2001) 1049–1054.
[15] J. Tan, W.M. Saltzman, Biomaterials 23 (2002) 3215–3225.
[16] J.B. Recknor, J.C. Recknor, D.S. Sakaguchi, S.K. Mallapragada, Biomaterials 25 (2004) 2753–2767.
[17] N. Maruyama, T. Koito, J. Nishida, T. Sawadaishi, X. Cieren, K. Ijiro, O. Karthaus, M. Shimomura, Thin solid films 327–329 (1998) 854–856.
[18] O. Karthaus, N. Maruyama, X. Cieren, M. Shimomura, H. Hasegawa, T. Hashimoto, Langmuir 16 (2000) 6071–6076.
[19] M. Tanaka, M. Takebayashi, M. Miyama, J. Nishida, M. Shimomura, Bio-med. Mater. Eng. 14 (2004) 439–445.
[20] H. Yabu, M. Shimomura, Adv. Funct. Mater. 15 (2005) 575–581.
[21] J. Nemoto, Y. Uraki, T. Kishimoto, Y. Sano, R. Funada, N. Obata, H. Yabu, M. Tanaka, M. Shimomura, Biores. Technol. 96 (2005) 1955–1958.
[22] R.D. Deegan, O. Balajin, T.F. Dupont, G. Huber, S.R. Nagel, T.A. Witten, Nature 389 (1997) 827–830.
[23] M. Nonomura, R. Kobayashi, Y. Nishiura, M. Shimomura, J. Phys. Soc. Jpn. 72 (2003) 2468–2471.
[24] E. Stepien, J. Stanisz, W. Korohoda, Cell Biol. Int. 23 (1998) 105–116.
[25] N.M. Dowell-Mesfin, M.A. Abdul-Karim, A.M.P. Turner, S. Schanz, H.G. Craighead, B. Roysam, J.N. Turner, W. Shain, J. Neural. Eng. 1 (2004) 78–90.
[26] E. Zamir, B. Geiger, J. Cell Sci. 114 (2001) 3583–3590.
[27] C.Y. Xu, R. Inai, M. Kotaki, S. Ramakrishna, Biomaterials 25 (2004) 877–886.
[28] Y. Fukuhira, E. Kitazono, T. Hayashi, H. Kaneko, M. Tanaka, M. Shimomura, Y. Sumi, Biomaterials 27 (2006) 1797–1802.
[29] M. Tanaka, K. Nishikawa, H. Okuba, H. Kamachi, T. Kawai, M. Matsushita, S. Todo, M. Shimomura, Colloids Surf. A. 284–285C (2006) 464–469.
[30] H. Sunami, E. Ito, M. Tanaka, S. Yamamoto, M. Shimomura, Colloids Surf. A. 284–285C (2006) 548–551.

Available online at www.sciencedirect.com
ScienceDirect
Surface Science 600 (2006) 3785–3791
SURFACE SCIENCE
www.elsevier.com/locate/susc

Relationship between adsorbed fibronectin and cell adhesion on a honeycomb-patterned film

Sadaaki Yamamoto [a,b,*], Masaru Tanaka [a,b], Hiroshi Sunami [a,b], Keiko Arai [c], Aiko Takayama [b], Shigeko Yamashita [b], Yuka Morita [a], Masatsugu Shimomura [b,c,d]

[a] *Creative Research Initiative "Sousei" (CRIS), Hokkaido University, N21W10 Kita-ku, Sapporo 001-0021, Japan*
[b] *Core Research for Evolutional Science and Technology (CREST), Japan Science and Technology Agency (JST), Honchou 4-1-8, Kawaguchi 332-0012, Japan*
[c] *Spatio-Temporal Function Materials Research Group, Frontier Research System, RIKEN Institute, 1-12 Hirosawa, Wako, Saitama 351-0198, Japan*
[d] *Nanotechnology Research Center, Research Institute for Electronic Science, Hokkaido University, N12W6 Kita-ku, Sapporo 060-0812, Japan*

Available online 21 April 2006

Abstract

Substratum surface morphology plays a vital roles in cellular behavior. Here, we characterized adsorption of fibronectin (Fn) as a typical cell adhesion protein onto honeycomb-patterned films made of poly(ε-caprolactone) (PCL) by using atomic force microscopy (AFM) and confocal laser scanning microscopy (CLSM). In order to determine how cells adhere to a honeycomb-patterned film, focal adhesion of cardiac myocytes (CMYs) and endothelial cells (ECs) on the films were studied by using fluorescence labeling of vinculin. Fn adsorbs around the pore edges to form ring-shaped structures. CMYs and ECs adhere onto the honeycomb-patterned films at focal contact points localized around pore edges distributed over the entire cellular surface. The focal contact points on the honeycomb-patterned films correspond well with the adsorption sites of Fn. We suggest that the cell response to honeycomb-patterned films is associated with the adsorption pattern of Fn on the film.

Keywords: Atomic force microscopy; Scanning electron microscopy; Cell adhesion; Adsorption; Self-assembly; Surface topography; Fibronectin; Tissue engineering

1. Introduction

Tissue engineering aims to restore, maintain, or improve complex human tissue function by using synthetic and living components [1]. Cells and the development of cytokines and scaffolds (cell-culture substrates) are key issues in tissue engineering. Since the original report that cells react to surfaces [2], cell response to material surfaces has been an intriguing topic in tissue engineering. Extensive research has documented that surface properties such as chemistry, charge, rigidity, and topography play vital roles in cellular behavior, such as adhesion, spreading, migration, proliferation, and differentiation. Recently, cell culture substrates with geometric micro- and nano-patterns have been fabricated by various methods and have been extensively used to investigate how cells respond to surface topography [3–24]. Although the effects of nano- and micro-patterned topography on cell responses have been well documented, the mechanisms behind these effects remain unresolved.

Fibronectin (Fn) is representative of a class of important cell adhesion proteins that are found in blood and associated with cell surfaces [25]. When adsorbed onto biomaterials, Fn undergoes a conformational change from a globular structure to extended structure, depending on surface properties such as surface charge, hydrophobicity, hydrophilicity, and plays a critical role in mediating cell responses. To determine the role of Fn in mediating cell

* Corresponding author. Address: Creative Research Initiative "Sousei" (CRIS), Hokkaido University, N21W10 Kita-ku, Sapporo 001-0021, Japan. Tel.: +81 11 706 9255; fax: +81 11 706 9291.
E-mail address: syama@cris.hokudai.ac.jp (S. Yamamoto).

0039-6028/$ - see front matter © 2006 Elsevier B.V. All rights reserved.
doi:10.1016/j.susc.2006.01.085

responses, adsorption of Fn both in molecularly isolated and aggregated states has been extensively investigated on various kinds of substrates, such as silica [26], methylated silica [26], mica [26,28], titanium [27], poly(methylmethacrylate) [28], sulfonated polystyrene [29], and glass [30] by using AFM, scanning electron microscopy (SEM), and fluorescence resonance energy transfer. Although adsorption of Fn is thus well-documented, little is known about the effect of substratum surface nano- and micropattern roughness on such adsorption [31].

Studies using biochemical methods suggest that structural changes in cell adhesion proteins such as fibronectin during adsorption onto a substrate determined by topography affect the molecular binding sites of these proteins to a receptor in cells, and thus affect the biological performance of these proteins and, ultimately, their critical role in mediating cell behavior [32,33]. Therefore, the correlation between the structures of adsorbed protein molecules and the substratum surface properties has been extensively researched. A detailed clarification of the effect of surface topography on protein adsorption requires a separation of the topographical and chemical effects, and, thus, requires a nano- and micro-fabrication method to form geometrical patterns with no variation in surface chemical properties. We have previously reported that honeycomb-patterned porous polymer films can be prepared by simple casting of polymer solutions of a water-immiscible solvent under high humidity (about 80% relative humidity at 21 ± 1 °C) [11–13,21,34–36]. The pore size of the films can be controlled over a wide range, from hundreds of nanometers to hundreds of microns. By mechanical stretching a honeycomb-patterned film made of a viscoelastic polymer, pores of various shapes, such as hexagonal, elongated hexagonal, rectangular, square-like, or triangle-like, can be formed in a controlled way [24]. Our recent studies on the culture of cells, such as endothelial cells (EC), cardiac myocytes (CMYs), neural projenitor cells, and hepatocytes, on honeycomb-patterned films revealed that cellular behavior such as migration, spreading, and morphology can be controlled by the size and shape of pores of the film [11,13,19,21,24]. These characteristics of honeycomb-patterned films make these films suitable candidates for cell-culture substrates used in studying the effect of substratum surface morphology on the adsorption of adhesive proteins and the role that morphology plays in cell behavior.

On honeycomb-patterned films, the conformational change in adhesion protein molecules such as fibronectin required for focal contact adhesion is supposedly the mechanism behind this control. In this study, the effect of surface morphology on the structure of adsorbed Fn was assessed by using atomic force microscopy (AFM) and confocal laser scanning microscopy (CLSM). Further, in order to determine how cells adhere to a honeycomb-patterned film, focal adhesion of cardiac myocytes (CMYs) and endothelial cells (ECs) on the films were studied by using fluorescence labeling of vinculin. The results showed that the structure of adsorbed Fn depends on the surface morphology of the films. Based on the structure of adsorbed Fn, the focal contact points of both types of cells on a honeycomb-patterned film are probably determined by the structure of Fn, leading to the characteristic biological response of a honeycomb-patterned film different from that of a flat film.

2. Experimental section

2.1. Materials

PCL and an amphiphilic copolymer (hereafter called Cap) of dodecylamide and ω-carboxyhexylacrylamide were used in the film fabrication. PCL (Wako) has a molecular weight of 70,000–100,000. Cap was synthesized by a method previously reported [37]. Fn was a bovine plasma fibronectin (lyophilized from 0.05 M tris-buffer saline, pH7.5) purchased from Sigma. Water was purified using a Millipore system (Milli-Q, Millipore). Benzene, chloroform, and 10% formalin solution (Wako) were used without further purification.

2.2. Film preparation

Honeycomb-patterned porous films (hereafter called honeycomb films) were fabricated on cover glasses ($\varphi =$ 15 mm, Matsunami Glass Industry, Japan) by a method previously reported [24,34–36].

2.3. Adsorbed Fn assay

The quantity of adsorbed Fn onto the films was determined for different coating concentrations using bicinconic acid (BCA) as protein assay reagent (Pierce, IL) [29]. Different concentrations of Fn (0–1000 μg/ml) were adsorbed in 24-well tissue culture plates (Iwaki, Japan) for 24 h at 37 °C in 5% CO_2. The Fn solutions were removed from the plates, and then the films were washed two times in PBS. The reaction started at 37 °C after working reagent at 200 μl/well was added. After incubation for 2 h, 160 μl of the Fn solution was transferred into a 96-well plate for reading by a microplate reader (BiotrakII, Biochrom Ltd., UK) at the 590-nm wavelength.

2.4. AFM, CLSM, and SEM measurements

Tapping-mode AFM imaging was performed under ambient conditions using a Digital Instrument Nanoscope IIIa Multimode system (Digital Instrument, Santa Barbara, CA) equipped with silicon nitride tips. The tips had a resonance frequency of ~300 kHz and a force constant of 14 N/m. The scan rate was 0.1–0.2 Hz, and the proportional and integral gains were set in the range of 2–10. CLSM measurements were performed using a CLSM apparatus (FLUOVIEW FV300, Olympus). The SEM images were obtained using a Hitachi S-3500N SEM

(Hitachi, Japan) at an acceleration voltage of 15 kV. A 200-μl aliquot of 240 μg/ml bovine plasma Fn (Sigma, Munich, Germany) in phosphate-buffered saline (PBS) was added to each honeycomb film and then incubated at 37 °C in 5% CO_2. The Fn-coated films were then gently washed with PBS, fixed with 10% formaldehyde (Wako) for 10 min at room temperature, permeabilized in PBS containing 1% normal goat serum and 0.1% Triton X-100 for 30 min, and then the film was incubated for 1 h with anti-Fn antibody (diluted 1:500; Sigma). After being rinsed with water, the films were treated with fluorescein isothiocyanate (FITC)-conjugated anti-rabbit IgG antibody (diluted 1:2000). The specimens for SEM were sputter-coated with Au–Pd using a sputter-coating unit (Hitachi E1030, Hitachi, Japan).

2.5. Cell culturing

CMYs were isolated by enzyme treatment of minced heart tissues of 19-day rat embryos (Sprague Dawley rats, Japan SLC, Inc.) [38]. CMYs were seeded onto the pre-fabricated cell-culture substrates (i.e., a flat film and a self-supported honeycomb film) at a density of 1.0×10^5 cells/cm^2. Culture medium pre-warmed at 37 °C (Hepes-buffered Hams F10 containing 0.5% ITS and 3% FCS) was replaced daily. One day and three days after seeding, vinculin of CMYs was stained as follows. Cells were fixed by immersion in 4% paraformaldehyde (SIGMA) solution for 10 min and permeabilized by immersion in 0.1% Triton X-100 (SIGMA) solution for 10 min. Cells were incubated for 1.5 h with mouse monoclonal anti-vinculin IgG_1 antibodies (CHEMICON International, Inc.) in 10% blocking solution (Dainippon Sumitomo Pharma) at 37 °C. After washing with PBS, vinculin complex were visualized by incubation with Alexa Fluor 488 anti-mouse IgG antibodies (Molecular Probe) for 1 h at 37 °C.

Porcine aortic endothelial cells (ECs, CSC Certificate™ Dainippon Pharmaceutical Co. Ltd.) were purchased. After the frozen cells were thawed at 45 °C, they were resuspended into a culture medium (Dulbecco's Modified Eagle's Minimal Essential Medium, SIGMA) containing 10% FBS, 100 unit/ml penicillin, and 100 μg/ml streptomycin. A honeycomb film and a flat film on glass plates were pre-incubated in the culture medium for 72 h at 37 °C in 5% CO_2 before cell seeding. ECs (passage number of 6–8) were seeded on the films at a density of 1.5×10^4 cells/cm^2. Culture medium was replaced after days 1, 3, 5, and 7. To visualize the focal adhesion, vinculin was stained by using an immunological method with primary antibodies (diluted 1:100, CHEMICON) and fluorescence-labeled secondary antibodies (diluted 1:1000, Alexa Fluor 546 goat anti-mouse IgG, Molecular Probes). For immunostaining, cells were fixed by immersion in 10% formalin (Wako) at 20 °C for 10 min and permeated with 1% PBS solution of Triton X-100 for 5 min at 20 °C.

3. Results and discussion

Fig. 1 shows SEM images of the structure of the PCL honeycomb film. The top-view image (Fig. 1a) reveals a well-arranged hexagonal lattice. The side-view image (Fig. 1c) reveals that the honeycomb films were porous with a double-layered structure in which two hexagonal lattices were connected vertically by pillars at the vertex of hexagons. A schematic model of this double-layered structure is shown in Fig. 1d.

The amount of Fn adsorbed on both the flat and honeycomb films was measured as a function of incubation time and of Fn-coating concentration determined by using a total adsorbed protein assay. The amount of Fn adsorbed on both films increased linearly with incubation time up to 1 h, and then became saturated. With increasing Fn-coating concentration up to 50 μg/ml, Fn adsorption on the flat film increased drastically and then saturated when the Fn-coating concentration reached 600 μg/ml. Although the adsorption behavior on the honeycomb films was similar to that on the flat films, the amount of Fn adsorbed on the honeycomb films was twice that on the same size of flat

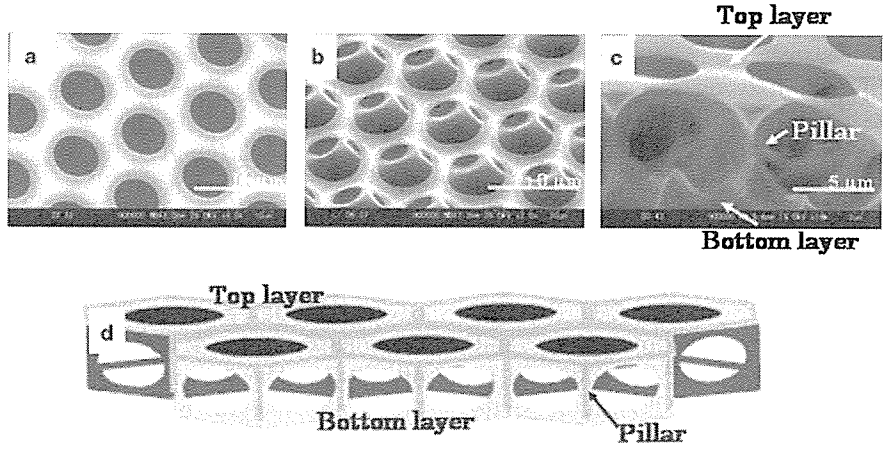

Fig. 1. SEM images of a honeycomb-patterned film. (a) Top view, (b) tilted view, (c) side view, and (d) schematic of the double-layered structure of the film.

films. Considering the three-dimensional porous structure of the honeycomb films (Fig. 1), the higher amount of adsorbed Fn might be due to the larger surface area of the film. This possibility is supported by the depth profile of the fluorescence intensity from stained Fn obtained by scanning excitation laser light from top to bottom of the films in CLSM. In the depth profile, fluorescence was observed only at the top and bottom surfaces of the honeycomb films and not within the film (data not shown), suggesting that Fn adsorbed onto the top (front and rear sides of the top layer) and bottom layer of a honeycomb film. Because the ratio of pore area to total surface area (porosity) of a top sheet is about 0.5, the estimated surface area of a honeycomb film for Fn adsorption is about twice that of a flat film, and thus the amount of Fn adsorbed on a honeycomb film should be about twice that on a flat film. The amount of adsorbed Fn at saturation on a flat film was 0.52 μg and that on a honeycomb film was 0.91 μg. The surface density at saturation on a flat film calculated using the surface area of a flat film (1.32 cm^2) and the adsorbed amount (0.52 μg) was about 0.4 $\mu g/cm^2$. This value agrees well with the approximate amount of Fn required for monolayer coverage, namely, 0.32 $\mu g/cm^2$, based on reported estimates of the dimension of a Fn molecule [32,33,39,40]. Based on the estimated surface area of a honeycomb film (twice the surface area of a flat film), the surface density of Fn on a honeycomb film is equal to that on a flat film. The total adsorbed protein assay revealed a monolayer-level adsorption behavior of Fn on both the flat and honeycomb films.

Fig. 2a shows AFM images of the surface of a flat film at 48 h incubation in 240 μg/ml Fn/PBS solution at 25 °C. Despite the monolayer-level adsorption, the surface was not uniform but had an interconnected fibrillar structure. Typical fibrils reached 30–50 μm in length, 0.5–2 μm in width, and 0.05–0.2 μm in height (AFM image shown in Fig. 2b). The CLSM image of stained Fn adsorbed on the flat films revealed a fibrillar structure similar to that revealed by AFM (Fig. 2c). Both images indicate that Fn adsorbs on the flat films to form aggregates with a fibrillar structure, similar to that of Fn adsorbed onto sulfonated polystyrene films [29], supporting our assignment that the fibril-like aggregates are adsorbed Fn.

Both CLSM and AFM images reveal that adsorption structure of Fn on a honeycomb film depend on incubation time up to 48 h (Fig. 3). Both images show that the surface of the honeycomb film after incubation in Fn/PBS solution completely differs from that of a flat film and depends on the incubation time. At an incubation time of 0 h, the surface is flat. At 20 h incubation, distinctly different morphologies coexist on the surface (AFM image in Fig. 3b); the surface above the dashed line in Fig. 3b is covered by numerous globules, whereas the surface below the dashed line is uniform. The distribution of the fluorescence from stained Fn in the CSLM image corresponds well to the morphological differences observed in the AFM image (Fig. 3c). By 48 h incubation, a few globules remain, and ring structures about 100 nm high and 1 μm wide appear around the pores as a dominant structure. Several rings were scraped off while repeating the tip scanning (as shown by white arrows in Fig. 3d,e). The CLSM image (Fig. 3h) reveals strong ring-like fluorescence along the pore edges, corresponding well to the ring structures evident in the AFM images (Fig. 3f). AFM image reveals that the surface

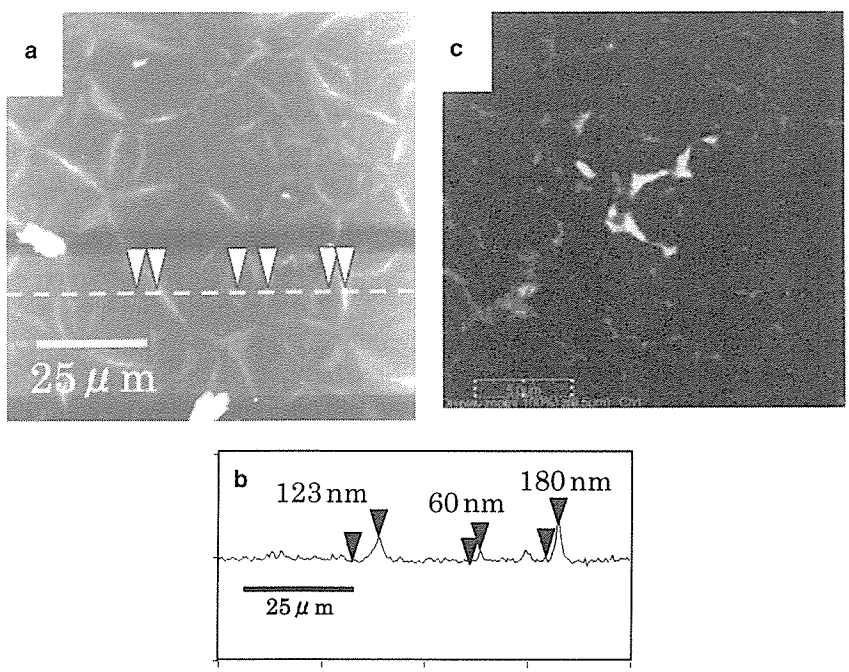

Fig. 2. (a) Topographic AFM image, (b) cross-sectional profile along the dotted line in (a), and (c) CLSM image of Fn adsorbed on a flat film observed after 48 h incubation in 1 ml of 240 μg/ml Fn/PBS solution at 25 °C.

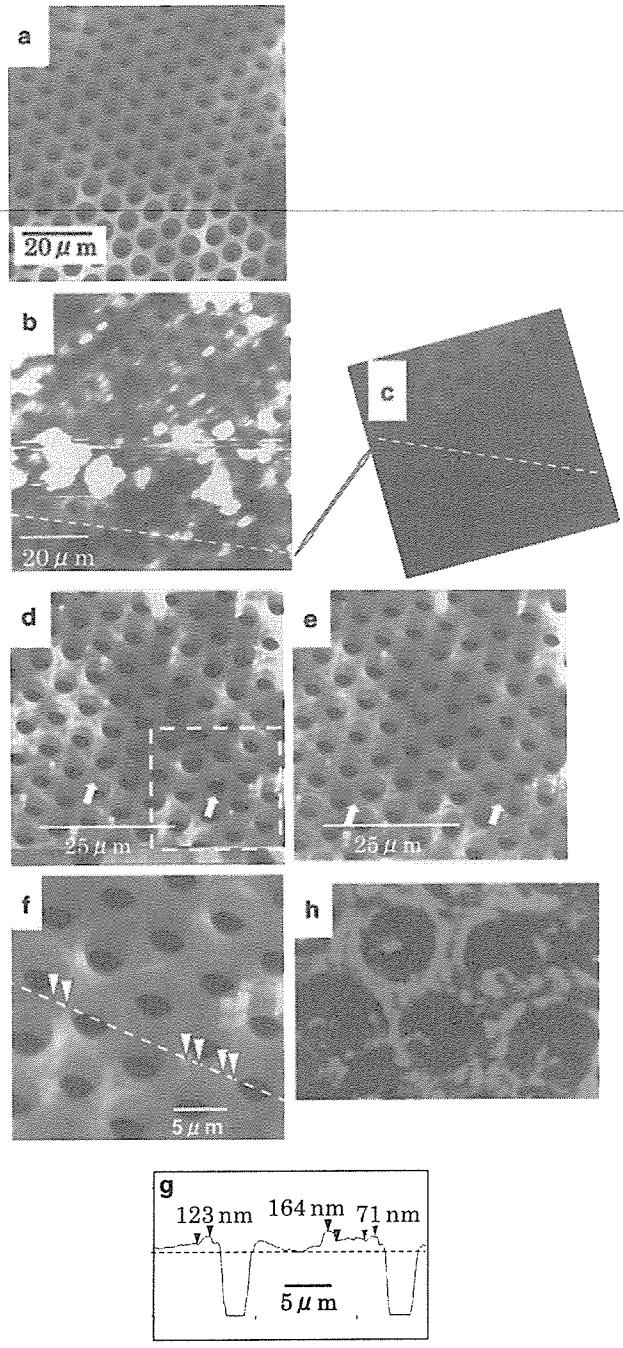

Fig. 3. AFM and CLSM images showing the morphology of adsorbed Fn as a function of incubation time in a PBS solution of Fn. (a) AFM image at 0 h incubation time. (b) AFM. (c) CLSM images at 20 h incubation time. Dashed line indicates the boundary separating two domains where morphology and fluorescence intensity differ. (d) AFM image at 48 h incubation time. (e) AFM image of surface after several scans on the surface of (d), where ring-like structures were scraped off by the scanning (compare areas indicated by white arrows in (d)). (f) Close-up image of area enclosed by dashed line in (d). (g) Cross-sectional profile along dotted line in (f). (h) CLSM image at incubation time of 48 h.

of the honeycomb films incubated in PBS solution between 0 and 48 h without Fn is uniform, and shows no evidence of any adsorbates. Both AFM and CLSM images reveal that Fn adsorbed and underwent a structural transition from globular form on the rim of the film to ring form around the edges of pores. A similar time-dependent self-organization of Fn has been reported for adsorption of Fn onto a sulfonated polystyrene surface [29], although the amount of adsorbed Fn was much higher than that for the honeycomb films used in our study.

The amount of adsorbed Fn on both films remains relatively constant, regardless of incubation time (longer than 1 h). Furthermore, the morphologies of the aggregates depend on the substrate surface structure (note that the chemical composition of both the honeycomb films and flat films was the same). Because protein molecules bound to a surface can rearrange via conformational changes [41] and diffusion [42], three-dimensional aggregate formation is possible, even for molecules adsorbed irreversibly with random orientations without overlapping or closed-packed monolayer density [43]. The structural transition from globular form to fibrillar form can be ascribed to the self-organization of adsorbed Fn caused by the dependence of diffusion on the surface morphology (honeycomb pattern and flat surface). Protein organization on a patterned surface has been reported for Fn adsorption onto Au/Si micro-patterns coated by a sulfonated polystyrene film [31]. Fn was adsorbed on the Si regions of the substrate but was repulsed by the Au domains, resulting in a structure of self-assembling Fn determined by the width of Si domains. The possible mechanism behind this Fn organization on the patterned surface is the balance between the bending energy of Fn and the unfavorable energy of contact with the Au interface. In our current study, the width of a rim of a honeycomb film on which Fn adsorbed was about 5 μm. The width of a rim and the size of a pore are comparable to the width of Si and Au domains of Au/Si micro-patterns (several microns to 20 μm). If pores play a role similar to the role that Au domains play, namely, that Fn does not adsorb, the same mechanism might be responsible for the self-organization of Fn on a honeycomb film.

To determine how cells adhere to a honeycomb film, vinculin within focal adhesions and actin cytoskeleton linked to integrin receptor in cell membranes were examined here by using immunofluorescence staining (Fig. 4). The focal contact points on a flat film clearly depend on the cells; EC adheres onto a flat film at cell peripheries and focal adhesions are very faint, whereas the focal contact points of CMYs are located randomly over entire cell bodies and the focal adhesions are strongly evident. Focal adhesion differs significantly between the honeycomb films and flat film. On the honeycomb films, focal adhesions of both types of cells are distributed over the entire cellular surface and located around the edges of pores lying beneath the cell bodies. Focal adhesion formation and subsequent actin polymerization are essential to a cell's ability to adhere. Integrin receptors recognize a specifically distinct peptide sequence of Fn (cell-binding RGD integrin recognition motif) that mediates cell-substrate focal contact adhesion. Binding of adhesion receptors to adsorbed Fn

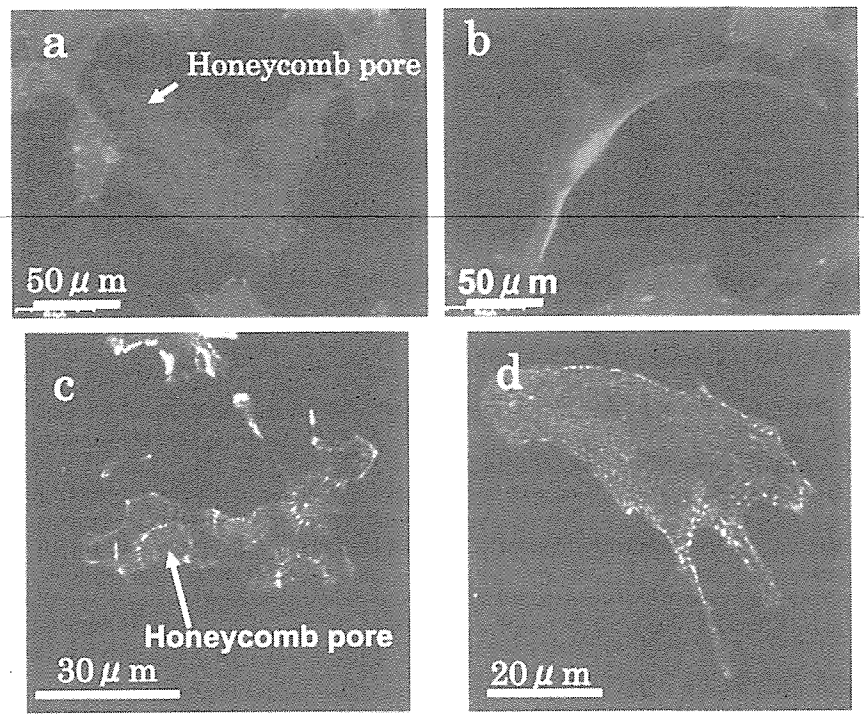

Fig. 4. CLSM images of (a) endothelial cells (ECs) (shown in red) and cardiac myocytes (CMYs) (shown in green) immunofluorescence stained for vinculin (focal contacts) on honeycomb-patterned film and flat film after 72 h incubation. (a) and (c) on a honeycomb film, (b) and (d) on a flat film. Locations of focal contact points around the edges of pores are clearly evident.

provides mechanical coupling to the underlying substrate and activates signal transductive pathways that control cellular behavior such as proliferation and differentiation [44]. The location of focal contact points corresponds well with the adsorption sites of Fn, suggesting that the focal adhesion pattern on honeycomb films is determined by the adsorption pattern of Fn. Focal contact points are regularly aligned on the honeycomb films. This adhesion pattern implies that the distance between adjacent focal contact points and/or the density of focal contact points are determined precisely by the pore size, and this distance and/or density might play a vital role in activating the signal transductive pathways. This control of focal contact points by the pore size might be an origin of the pore-size dependence of cell response characteristics to a honeycomb film.

4. Summary

In this study, the adsorption structure of Fn and the adhesion patterns of ECs and CMYs on honeycomb films and flat films was studied, and the role the honeycomb film plays on cell response were discussed. Results showed that the structure of adsorbed Fn was determined by the micro-pattern pores of the honeycomb film and by incubation time. The structure of adsorbed Fn changed with increasing incubation time from globular to fibril-like form. The fibril-like aggregates were located on the periphery of micro-pores. The focal contacts of the cells located on the periphery of the micro-pores are apparently determined by the fibril-like form of adsorbed Fn. We suggest that the cell response to the honeycomb-patterned film is associated with the ordered adsorption pattern of Fn on the honeycomb film, leading to the characteristic response of a honeycomb film different from that of a flat film. The results presented here suggest a mechanism where the structure of the adsorbed cell adhesion proteins determined by a substrate micro-pattern affects the molecular binding sites of the proteins to a receptor in cells, affects the biological performance of the proteins and, thus ultimately affects their critical role in mediating cell behavior.

Acknowledgements

This study was supported by a Special Coordination Funds for Promoting Science and Technology, Ministry of Education, Culture, Sports, Science and Technology, Japan (Mext), CREST-JST (Grants-in-Aid from the Japan Science and Technology Corporation).

References

[1] R. Langer, J.P. Vacanti, Science 260 (1993) 920.
[2] A. Carrel, M. Burrows, J. Exp. Med. 13 (1911) 571.
[3] J.A. Hubbel, Biotechnology 13 (1996) 565.
[4] C.S. Chen, M. Mrksich, S. Huang, G.M. Whitesides, D.E. Ingber, Science 276 (1997) 1425.
[5] A.M. Green, J.A. Jansen, J.-P.C.M. van der Waerden, A.F. von Recum, J. Biomed. Mater. Res. 28 (1994) 647.
[6] S. Turner, L. Kam, M. Isaacson, H.G. Graighead, W. Shain, J. Turner, J. Vac. Sci. Technol. 15 (1997) 2848.

[7] A. Curtis, C. Wilkinson, Biomaterials 18 (1997) 1573.
[8] R.S. Kane, S. Takayama, E. Ostuni, D.E. Ingber, C.M. Whiteside, Biomaterials 20 (1999) 2363.
[9] E.T. den Braber, J.E. de Reijter, L.A. Ginsel, A.F. van Recum, J.A. Jansen, J. Biomed. Mater. Res. 40 (1998) 291.
[10] A. Folch, M. Toner, Biotechnology 14 (1998) 388.
[11] T. Nishikawa, J. Nishida, R. Ookura, S. Nishimura, S. Wada, T. Karino, M. Shimomura, Mater. Sci. Eng. C8-9 (1999) 495.
[12] T. Nishikawa, J. Nishida, R. Ookura, S. Nishimura, S. Wada, T. Karino, M. Shimomura, Mater. Sci. Eng. C10 (1999) 141.
[13] K. Sato, K. Hasebe, M. Tanaka, M. Takebayashi, K. Nischikawa, M. Schimomura, T. Kawai, M. Matsushita, S. Todo, Int. J. Nanosci. 1 (2002) 689.
[14] H.G. Graighead, C.D. James, A.M.P. Turner, Curr. Opi. Sol. State Mater. Sci. 5 (2001) 177.
[15] A. Mata, C. Boehm, A.J. Fleischman, G. Muschlar, S. Roy, J. Biomed. Mater. Res. 62 (2002) 499.
[16] M. Arnold, A.E. Cavalcanti-Adam, R. Glass, J. Blümmel, W. Eck, M. Kantlehner, H. Kessler, J.P. Spatz, Chem. Phys. Chem. 5 (2004) 383.
[17] X.F. Walboomers, L.A. Ginsel, J.A. Jansen, J. Biomed. Mater. Res 51 (2000) 529.
[18] N.M. Dowell-Mesfin, M.-A. Abdul-Karim, A.M.P. Turner, S. Scanz, H.G. Craighesd, B. Roysam, J.N. Turner, W. Shain, e-J. Neural Eng. 1 (2004) 78.
[19] A. Tsuruma, M. Tanaka, N. Fukushima, M. Shimomura, e-J. Surf. Sci. Nanotech. 3 (2005) 159.
[20] M.J. Dalby, M.O. Riehle, D.S. Sutherland, H. Agheli, A.S.G. Gurtis, J. Biomed. Mater. Res. 69A (2004) 314.
[21] T. Nishikawa, J. Nishida, R. Ookura, H. Ookubo, H. Kamachi, M. Matsushita, S. Todo, M. Schimomura, Stud. Surf. Sci. Catal. 132 (2001) 132, 509.
[22] F.A. Denis, P. Hanarp, D.S. Sutherland, J. Gold, C. Mustin, P.G. Rouxhet, Y.F. Dufrêne, Langmuir 18 (2002) 819.
[23] M.J. Dalby, S. Childs, M.O. Riehle, H.J.H. Johnstone, S. Affrossman, A.S.G. Curtis, Biomaterials 24 (2003) 927.
[24] T. Nishikawa, M. Nonomura, K. Arai, J. Hayashi, T. Sawadaishi, Y. Nishiura, M. Hara, M. Shimomura, Langmuir 19 (2003) 6193.
[25] R.O. Hynes, Fibronectin, Springer, New York, 1990, p. 546.
[26] M. Bergkvist, J. Carlsson, S. Oscarsson, J. Biomed. Mater. Res. 64A (2003) 349.
[27] D.E. MacDonald, B. Markovic, M. Allen, J. Biomed. Mater. Res. 41 (1998) 120.
[28] E.R. Zenhausen, M. Jobin, M. Taborelli, P. Descounts, Ultramicroscopy 42–44 (Pt B) (1992) 1155.
[29] N. Pernodet, M. Rafailovich, J. Sokolov, D. Xu, N.-L. Yamg, K.J. McLeod, Biomed. Mater. Res. 64A (2003) 684.
[30] L. Bough, V. Vogel, J. Biomed. Mater. Res. 69 (2004) 525.
[31] N. Pernodet, S. Lenny, J. John, R. Miriam, Amer. Phys. Soc., March Meeting 2004, 22–26 March 2004, Palais des Congress de Montreal, Montreal, Que., Canada, Meeting ID; MAR04, abstract#P9.011.
[32] A.G. Garcia, M.D. Vega, D. Boettinger, Mol. Biol. Cell 10 (1999) 785.
[33] A.G. Garcia, D. Boettinger, Biomaterials 20 (1999) 2427.
[34] N. Maruyama, T. Koito, J. Nishida, T. Sawadaishi, X. Gieren, K. Ijiro, O. Karthaus, M. Shimomura, Thin Solid Films 854 (1998) 327.
[35] T. Nishikawa, R. Okura, J. Nishida, K. Arai, J. Hayashi, N. Kurono, T. Sawadaishi, M. Hara, M. Schimomura, Langmuir 18 (2002) 5734.
[36] M. Tanaka, M. Takebayashi, M. Miyama, J. Nishida, M. Schimomura, Bio-Med. Mater. Eng. 14 (2004) 439.
[37] S. Nishimura, K. Yamada, J. Am. Chem. Soc. 119 (1997) 10555.
[38] M.C. Denyer, M. Riehle, M. Scholl, C. Sproessler, S.T. Britland, A. Offenhaeusser, W. Knoll, In Vitro Cell. Dev. Biol. Anim. 35 (1999) 352.
[39] F. Grinnel, M.K. Feld, J. Biomed. Mater. Res. 15 (1981) 363.
[40] E.C. Williams, P.A. Janmey, J.D. Ferry, D.F. Mosher, J. Biol. Chem. 257 (1982) 14973.
[41] W.G. Pitt, S.H. Spiegelberg, S.L. Cooer, in: J.L. Brash, T.A. Horbett (Eds.), Proteins at Interfaces Physicochemical and Biochemical Studies, ACS Symposium Series, Amer. Chem. Soc., Washington, DC, 1987, p. 324.
[42] R.D. Tilton, C.R. Robertson, A.P. Gast, J. Coll. Interface Sci. 137 (1990) 192.
[43] P.A. Dimilla, S.M. Albelda, J.A. Quinn, J. Coll. Interface Sci. 153 (1992) 212.
[44] K. Buridge, M. Charanowska-Wodnick, Ann. Rev. Cell Dev. Biol. 12 (1996) 463.